PAPER

Synthesis of efficient bi-anchoring bifuran/biphenyl derivatives for dye-sensitized solar cell applications†

Heba M. El-Shafeai, Safa A. Badawy, [ORCID] Mohamed A. Ismail, [ORCID] Ehab Abdel-Latif, Ahmed A. Fadda [ORCID] and Mohamed R. Elmorsy [ORCID] *

The synthesis, description, and demonstration of dye-sensitive solar cell sensitizers containing bifuran/biphenyl derivatives with cyanoacetic acid, barbiturate, thiobarbituric acid, and 4-carboxylcyanoacetamides have been reported. A photovoltaic performance measurement was conducted using the Ru(II) dye **N3** as a reference to examine the effects of different electron acceptor units and replacement of the π-spacer bifuran by biphenyl units on the photophysical, electrochemical, and photovoltaic properties of eight new distinct organic dyes **HB-1–8**. The new organic dyes **HB-1–8** were prepared and compared with the **N3** metal dye. Density functional theory calculations were carried out to explore the ground state geometrical structures and electronic structures of the eight dyes. Under standard global AM 1.5 solar condition, the solar cells based on **HB-1–8** show the overall power conversion efficiencies of 2.93–5.51%. The presented research shows that the organic dye photovoltaic performances can vary greatly depending on the type of electron donor and acceptor used. Dye **HB-3** exhibited the highest efficiency among the eight investigated dyes, reaching 5.51% with a V_{OC} value higher than **N3**.

1. Introduction

Solar power is the largest untapped resource for renewable energy on Earth. Due to its low price and versatility with superior cost-to-efficiency proportion, dye-sensitized solar cells (DSSCs) have been the subject of intensive research ever since their successful display by Grätzel and coworkers.[1] Numerous strategies have been pursued in recent decades to create efficient sensitizers with increasing photostability and conversion efficiency, converting sunlight to electricity.[2] While ruthenium-based dyes such as black dye, **N3**, and **N719** were used to sensitize the most effective devices, these chromophores are associated with a variety of drawbacks, including high cost, metal shortage, and time-consuming purification processes.[3–5] In contrast, organic dyes benefit from their simple structural modulation, low environmental impact, low cost, simplified synthesis, and outstanding light-harvesting expertise.[6] The sensitizer is a key component of DSSCs due to its role in absorbing photons and converting them into electrons through the cell. Because of its importance to DSSCs, its molecular structure should be carefully engineered to achieve wider panchromatic absorption spectra, appropriate FMO energy

levels, and outstanding stability.[7] According to this study, the donor–(π-spacer)–acceptor (D–π–A) strategy is the most widely studied molecular geometry for effective organic dyes.[8] The π-conjugation linkage between the donating portion and the acceptor unit facilitates effective photo-induced intramolecular charge transfer (ICT). Most of these dyes use electron-donating units derived from a variety of organic core structures, including indole, triarylamine, phenothiazine, and carbazole.[9] Furthermore, the presence of an additional electron-drawing unit (A) could significantly decrease the organic dye's HOMO–LUMO gap and thus improve its photostability. Several di-anchoring organic dyes designed and synthesized for use in DSSCs have demonstrated better cell performance than mono-anchoring D–π–A sensitizers, with an improved photocurrent due to the extension of the π-conjugated system and the increased molar extinction coefficient.[10] Because of its high optoelectronic efficiency, high conductivity potential, and high stability,[11] using furan and phenyl as donors is also generally accepted as a good way to improve the chemical, electrical, spectroscopic, and overall stability of the particles that will likely be made. In recent scientific literature, numerous dyes with multiple anchoring moieties were reported. Double-anchoring organic sensitizers have several advantages over single-anchoring sensitizers, including (i) a bathochromic shift in the absorption spectra, (ii) strong binding to the semiconductor, (iii) greatest stability, (iv) increased number of the injected protons.[12–14] To produce more potent DSSCs, the

Department of Chemistry, Faculty of Science, Mansoura University, 35516 Mansoura, Egypt. E-mail: m.r.elmorsy@mans.edu.eg; m.r.elmorsy@gmail.com

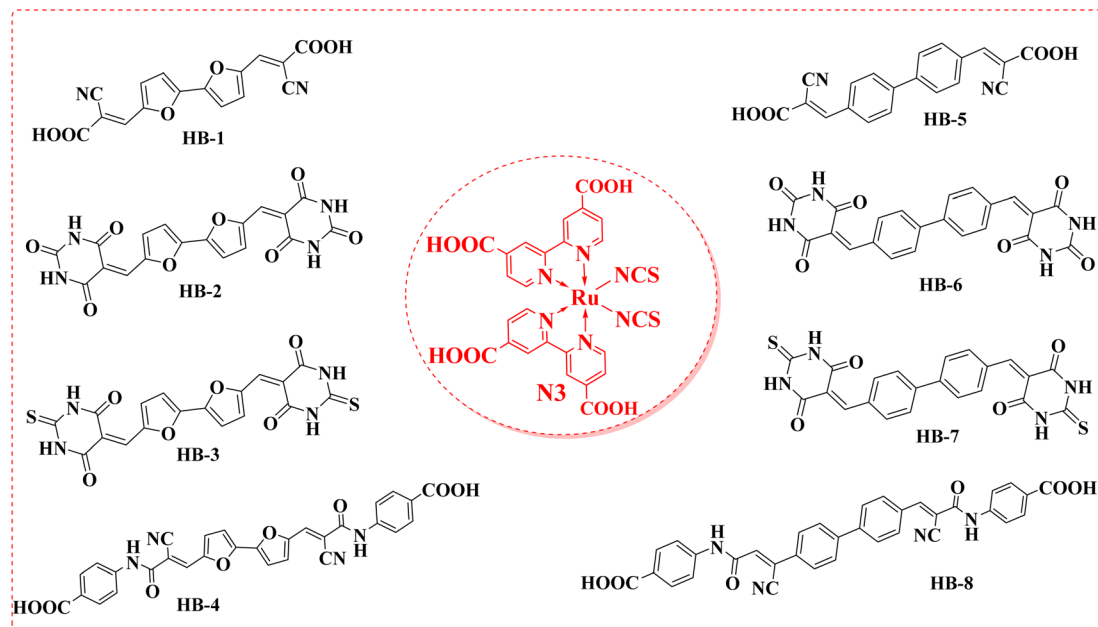† Electronic supplementary information (ESI) available. See DOI: https://doi.org/10.1039/d3ra00609c

Fig. 1 Chemical structures of sensitizers **HB-1–8** and **N3**.

architecture must be refined with double anchoring compounds. In comparison with their single counterparts, these compounds exhibit enhanced light-harvesting characteristics and are more stable.[15,16] Therefore, in this research article, we have explored the effectiveness of anchoring moieties such as barbituric acid, thiobarbituric acid and cyanoacetamide moieties in TiO$_2$-DSSCs. The newly designed sensitizer incorporates bifuran/biphenyl cores that are directly attached to cyanoacetic acid, barbituric acid, thiobarbituric acid and 4-carboxylcyanoacetamide acceptor units on two terminals. In our study, in comparison with the bifuran/biphenyl dyes **HB-1–8** with the metal complex dye **N3**, **HB-3** with double thiobarbituric acid units as the anchor group exhibited the best overall conversion efficiency with the simultaneous enhancement of photocurrent and photovoltage. Fig. 1 exhibits the molecular structures of **HB-1–8** and Ru(II) dye **N3**.

2. Experimental section

2.1. Materials and methods

Materials and methods are discussed in detail in the ESI.† All devices, equipment and fabrication for DSSCs are also shown in the ESI.†

2.2. Structural interpretation

HB-1–8 was analyzed using IR, ^{1}H NMR, and ^{13}C NMR spectra. As a result, Fig. S1–S29 (ESI†) contain their related figures.

2.3. Synthetic procedures

2.3.1 General methodology for the preparation of [2,2′-bifuran]-5,5′-diylbis(methanylylidene)bis(pyrimidine) derivatives. The preparation of [2,2′-bifuran]-5,5′-diylbis(methanylyli-dene)bis(pyrimidine) derivatives **HB-1–4** started with treatment

of 5-bromofuran-2-carbaldehyde (**1**) (950 mg, 5.4 mmol), with (5-formylfuran-2-yl)boronic acid (**2**) (909 mg, 6.5 mmol), and a catalytic amount of Pd(PPh$_3$)$_4$ with 4 g K$_2$CO$_3$ in 25 mL of dioxane as a solvent. The reaction mixture was refluxed for 10–12 h, and then it was extracted with ethyl acetate. The extracted organic layer was evaporated, and the solid formed was purified by recrystallization using a mixture of ethyl acetate and toluene to afford 2,2′-bifuran-5,5′-dicarbaldehyde (**3**) mp = 264–266 °C, lit.[17] mp = 264–265 °C. Bifuran-dialdehyde **3** (114 mg, 0.6 mmol) was reacted with 2-cyanoacetic acid (**4**) (127 mg, 1.5 mmol), barbituric acid (**5a**) (192 mg, 1.5 mmol) and 2-thiobarbituric acid (**5b**) (216 mg, 1.5 mmol) in 25 mL of methyl alcohol and acetic acid, and 4-(2-cyanoacetamido)benzoic acid (**6**) (306 mg, 1.5 mmol) in 25 mL of ethyl alcohol and drops of piperidine. The mixture was refluxed for 10–12 h and the formed solid was collected while hot, recrystallized from ethyl acetate–DMF, and dried to obtain the targeted compounds **HB-1**, **HB-2**, **HB-3** and **HB-4**.

*3-(5′-(2-Carboxy-2-cyanovinyl)-[2,2′-bifuran]-5-yl)-2-cyanoacrylic acid (**HB-1**).* Compound **HB-1** (76% yield, red ppt), mp = >360 °C, IR (KBr) ν'/cm^{-1}: 3423 (OH, stretch), 3149, 3093 (CH, stretch), 2228 (CN, stretch), 1728 (C=O, stretch), 1593, 1511, 1437 (C=C, stretch). ^{1}H-NMR (DMSO-d_6) δ 7.13 (d, J = 4.00 Hz, 2H, furan-H's), 7.62 (d, J = 4.00 Hz, 2H, furan-H's), 8.12 (s, 2H), 13.88 (s, 2H, carboxylic-H's). ^{13}C-NMR; δ 99.61 (2C), 112.66 (2C), 115.98 (2C), 125.43 (2C), 137.58 (2C), 148.12 (2C), 149.14 (2C), 163.44 (2C) ppm. MS (EI) m/z (rel. int.) C$_{16}$H$_8$N$_2$O$_6$ (324.25); 324.25 (M$^+$, 49.31), 136.23 (100). Anal. calcd. For C$_{16}$H$_8$N$_2$O$_6$ (324.25): C, 59.27; H, 2.49; N, 8.64. Found. C, 59.31; H, 2.58; N, 8.49.

*5,5′-([2,2′-Bifuran]-5,5′-diylbis(methanylylidene))bis(pyrimidine-2,4,6(1H,3H,5H)-trione) (**HB-2**).* Compound **HB-2** (82% yield, red ppt), mp = >360 °C, IR (KBr) ν'/cm^{-1}: 3214 (NH, stretch), 3073 (CH, stretch), 1741, 1703, 1671 (C=O, stretch), 1566 (C=C,

stretch), ^{1}H-NMR (DMSO-d_6) δ 7.52 (d, J = 4.00 Hz, 2H, furan-H's), 8.04 (s, 2H), 8.57 (d, J = 4.00 Hz, 2H, furan-H's), 11.34 (s, 2H, 2× N–H), 11.41 (s, 2H, 2× N–H), MS (EI) m/z (rel. int.) $C_{18}H_{10}N_4O_8$ (410.3); 410.20 (M$^+$, 2.66), 262.20 (91.99), 57 (100). Anal. calcd. For $C_{18}H_{10}N_4O_8$ (410.3): C, 52.69; H, 2.46; N, 13.66. Found. C, 52.54; H, 2.64; N, 13.45.

5,5′-([2,2′-Bifuran]-5,5′-diylbis(methanylylidene)) bis-(2-thio-xodihydropyrimidine-4,6(1H,5H)-dione) (HB-3). Compound **HB-3** (79%, deep red ppt), mp = >360 °C, IR (KBr) v'/cm^{-1}: 3449 (NH, stretch), 3150, 3067 (CH, stretch), 1701, 1654 (C=O, stretch), 1535, 1513 (C=C, stretch), 1355 (C=S, stretch). ^{1}H-NMR (DMSO-d_6) δ 7.58 (d, J = 4.00 Hz, 2H, furan-H's), 8.03 (s, 2H), 8.62 (d, J = 4.00 Hz, 2H, furan-H's), 12.46 (s, 2H, 2× N–H), 12.52 (s, 2H, 2× N–H). ^{13}C-NMR; δ 114.40 (2C), 115.58 (2C), 129.04 (2C), 135.55 (2C), 149.71 (2C), 151.71 (2C), 159.92 (2C), 161.41 (2C), 178.20 (2C) ppm. MS (EI) m/z (rel. int.) $C_{18}H_{10}N_4O_6S_2$ (442.42); 442.44 (M$^+$, 15.27), 433.39 (100). Anal. calcd. For $C_{18}H_{10}N_4O_6S_2$ (442.42): C, 48.87; H, 2.28; N, 12.66. Found. C, 49.11; H, 2.43; N, 12.77.

4,4′-(3,3′-[2,2′-Bifuran]-5,5′-diyl)bis(2-cyanoacryloyl) bis(azanediyl)dibenzoicacid (HB-4). Compound **HB-4** (73% yield, deep red ppt), mp = >360 °C, IR (KBr) v'/cm^{-1}: 3405 (OH & NH, stretch), 2204 (CN, stretch), 1683 (C=O, stretch), 1594, 1525, 1437 (C=C, stretch). ^{1}H-NMR (DMSO-d_6) δ 7.17 (d, J = 4 Hz, 2H, furan-H's), 7.61–7.93 (m, 10H, Ar-H's), 8.21 (s, 2H, methine-H's), 10.63 (s, 2H, 2× N–H), 12.92 (s, 2H). MS (EI) m/z (rel. int.) $C_{30}H_{18}N_4O_8$ (562.49); 562.26 (M$^+$, 25.12), 338.22 (100). Anal. calcd. For $C_{30}H_{18}N_4O_8$ (562.49): C, 64.06; H, 3.23; N, 9.96. Found. C, 63.96; H, 3.11; N, 10.21.

2.3.2 General methodology for the preparation of [1,1′-biphenyl]-4,4′-diylbis(methanylylidene))bis-(pyrimidine) derivatives HB-5–8. [1,1′-Biphenyl]-4,4′-dicarbaldehyde (**9**) was prepared *via* Suzuki coupling reaction of 4-bromobenzaldehyde (**7**) (1 g, 5.4 mmol) with (4-formylphenyl)boronic acid (**8**) (955 mg, 6.4 mmol), Pd(PPh$_3$)$_4$ as a catalyst (120 mg), and 4 g of anhydrous K$_2$CO$_3$ as a base in 25 mL of 1,4-dioxane. The reaction mixture was refluxed overnight, then it was extracted with ethyl acetate, and the organic layer was evaporated until the formation of solid product that was purified from ethyl acetate-toluene by recrystallization process to obtain [1,1′-biphenyl]-4,4′-dicarbaldehyde (**9**) mp = 148–149 °C, lit.[18] mp = 146–148 °C. Biphenyl dyes **HB-5–8** were prepared by the same methodology used for bifuran dyes **HB-1–4** using biphenyldialdehyde (**9**) instead of bifurandialdehyde (**3**).

3,3′-([1,1′-Biphenyl]-4,4′-diyl)bis(2-cyanoacrylic acid) (HB-5). Compound **HB-5** (81% yield, pale yellow ppt), mp = 296–298 °C, IR (KBr) v'/cm^{-1}: 3321 (OH, stretch), 3045 (CH, stretch), 2221 (CN, stretch), 1751 (C=O, stretch), 1604, 1541, 1495 (C=C, stretch). ^{1}H-NMR (DMSO-d_6) δ 7.22 (s, 2H, H's of carboxylic exchangeable with D$_2$O), 7.97 (d, J = 8.00 Hz, 4H, Ar-H's), 8.09 (d, J = 8.00 Hz, 4H, Ar-H's), 8.20 (s, 2H). ^{13}C-NMR; δ: 117.08 (2C), 127.56 (6C), 131.06 (4C), 131.95 (2C), 142.12 (2C), 151.63 (2C), 163.17 (2C) ppm, MS (EI) m/z (rel. int.) $C_{20}H_{12}N_2O_4$ (344.33); 344 (M$^+$, 27), 300 (M$^+$–CO$_2$, 100), 256 (M$^+$–2CO$_2$, 29). Anal. calcd. For $C_{20}H_{12}N_2O_4$ (344.33): C, 69.77; H, 3.51; N, 8.14. Found. C, 69.46; H, 3.58; N, 8.23.

5,5′-([1,1′-Biphenyl]-4,4′-diylbis(methanylylidene))bis(pyr-imidine-2,4,6(1H,3H,5H)-trione) (HB-6). Compound **HB-6** (74% yield, yellow ppt), mp = >360 °C, IR (KBr) v'/cm^{-1}: 3202 (NH, stretch), 3091 (CH, stretch), 1750, 1677 (C=O, stretch), 1572, 1493 (C=C, stretch), ^{1}H-NMR (DMSO-d_6) δ 7.92 (d, J = 8.0 Hz, 4H, Ar-H's), 8.24 (d, J = 9.00 Hz, 4H, Ar-H's), 8.31 (s, 2H, methine-H's), 11.27 (s, 2H, 2× N–H), 11.41 (s, 2H, 2× N–H), MS (EI) m/z (rel.int.) $C_{22}H_{14}N_4O_6$ (430.38); 430 (M$^+$, 2.5), 55 (100). Anal. calcd. For $C_{22}H_{14}N_4O_6$ (430.38): C, 61.40; H, 3.28; N, 13.02. Found. C, 61.28; H, 3.47; N, 12.87.

5,5′-([1,1′-Biphenyl]-4,4′-diylbis(methanylylidene))bis(2-thio-xodihydropyrimidine-4,6(1H,5H)-dione) (HB-7). Compound **HB-7** (70% yield, orange ppt), mp = >360 °C, IR (KBr) v'/cm^{-1}: 3451 (NH, stretch), 3223 (CH, stretch), 1674 (C=O, stretch), 1559, 1526, 1447 (C=C, stretch), 1415 (C=S, stretch). ^{1}H-NMR (DMSO-d_6) δ 7.96 (d, J = 8.50 Hz, 4H, Ar-H's), 8.31 (d, J = 8.80 Hz, 4H, Ar-H's), 8.35 (s, 2H, methine-H's), 12.40 (s, 2H, 2× N–H), 12.50 (s, 2H, 2× N–H), MS (EI) m/z (rel. int.) $C_{22}H_{14}N_4O_4S_2$ (462.5); 462.61 (M$^+$, 43), 455.99 (100). Anal. calcd. For $C_{22}H_{14}N_4O_4S_2$ (462.5): C, 57.13; H, 3.05; N, 12.11. Found. C, 57.46; H, 2.84; N, 12.34.

4,4′-(3,3′-([1,1′-Biphenyl]-4,4′-diyl)bis(2-cyanoacryloyl) bis(azanediyl))dibenzoic acid (HB-8). Compound **HB-8** (75% yield, golden yellow ppt), mp = >360 °C, IR (KBr) v'/cm^{-1}: 3369 (OH & NH, stretch), 2208 (CN, stretch), 1691 (C=O, stretch), 1593, 1524, 1405 (C=C, stretch). ^{1}H-NMR (DMSO-d_6) δ 7.75 (d, J = 8.50 Hz, 4H, Ar-H's of biphenyl ring), 7.92 (d, J = 8.00 Hz, 4H, Ar-H's of biphenyl ring), 8.06 (d, J = 9.00 Hz, 4H, Ar-H's of phenylacetamide ring), 8.13 (d, J = 9.00 Hz, 4H, Ar-H's of phe-nylacetamide ring), 8.38 (s, 2H, methine-H's), 10.77 (s, 2H, 2× N–H). MS (EI) m/z (rel. int.) $C_{34}H_{22}N_4O_6$ (582.57); 582.24 (M$^+$, 24.25), 159.66 (100). Anal. calcd. For $C_{34}H_{22}N_4O_6$ (582.57): C, 71.32; H, 3.92; N, 8.71. Found. C, 70.87; H, 3.79; N, 8.31.

3. Results and discussion

3.1. Synthesis

Bifuran structures **HB-1–3** (Scheme 1) were prepared *via* condensation reaction of 2,2′-bifuran-5,5′-dicarbaldehyde (**3**) with cyanoacetic acid (**4**), barbituric acid (**5a**), thiobarbituric acid (**5b**), in methanol–acetic acid as a solvent with reflux. Dye **HB-4** was prepared by refluxing dialdehyde **3** with 4-(2-cyanoa-cetamido)benzoic acid (**6**) in ethanol as a solvent and piperidine as a catalyst. The bifuran-dialdehyde **3** was made *via* a Suzuki coupling reaction of 5-bromofuran-2-carbaldehyde (**1**) with (5-formylfuran-2-yl)boronic acid (**2**). Structures of the newly synthesized dyes **HB-1–4** were assigned based on their elemental and spectral analyses. IR spectra of **HB-1** and **HB-4** displayed the stretching vibrations of nitrile groups at 2228 cm^{-1} (**HB-1**) and 2204 cm^{-1} (**HB-4**), plus OH stretching vibrations at 3423 cm^{-1} (**HB-1**) and 3405 cm^{-1} (**HB-4**/OH NH). The ^{1}H-NMR spectrum of **HB-1** showed the related protons of the furan ring at δ 7.13, as well as 7.62 ppm (two protons each) as two doublet signals with a coupling constant of J = 4.00 Hz, two singlet signals δ 8.12 (2H, methine-H's), δ 13.88 (2H, carboxylic-H's). The ^{13}C-NMR spectrum of **HB-1** displayed eight carbon signals with the characteristic carbon of the carboxylic
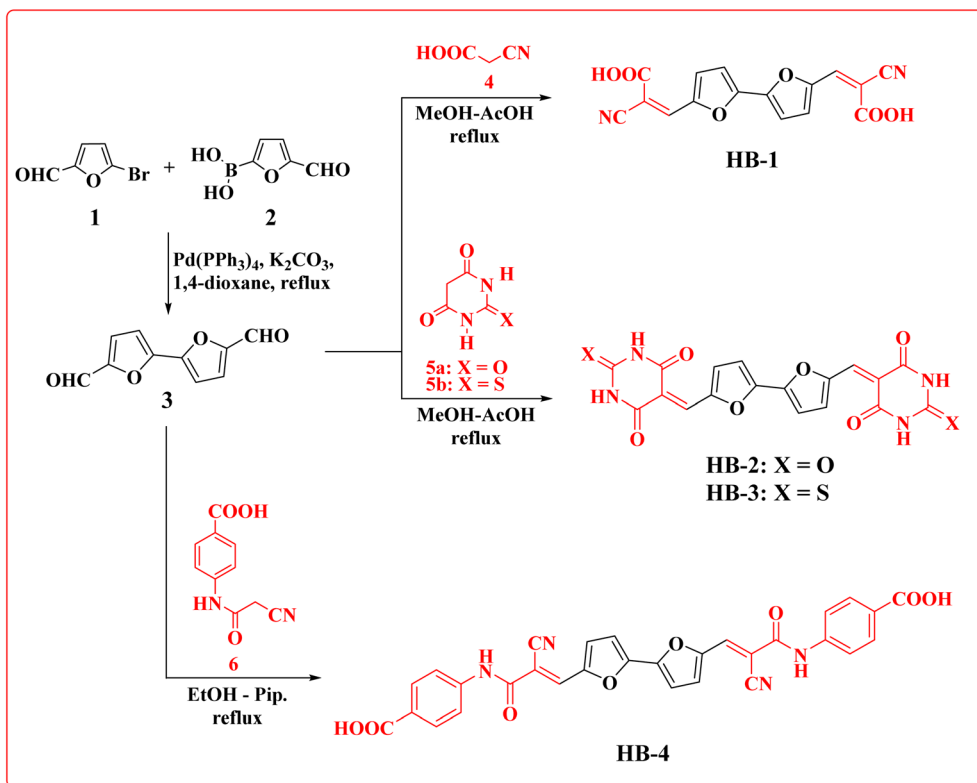
Scheme 1 Synthesis scheme of bifuran dyes **HB-1–4**.
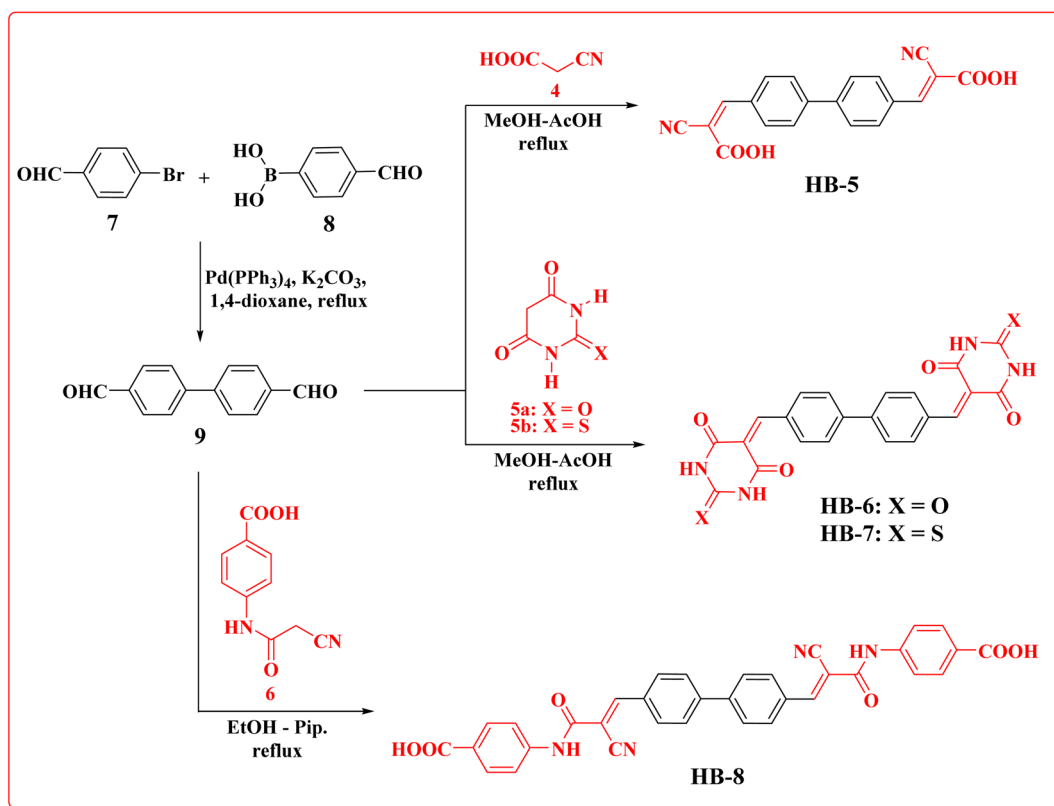
Scheme 2 Synthesis scheme of biphenyl dyes **HB-5–8**.

group at δ 163.44 ppm. Furthermore, MS of **HB-1** gave a peak m/z at 324.25, confirming its molecular weight. The ^{1}H-NMR spectrum of **HB-3** showed the related protons for the furan ring at δ 7.58 and 8.62 ppm (two protons each) with a coupling constant of $J = 4$ Hz, three singlet signals at δ 8.03 (2H, methine-H's), δ 12.46 (2H, 2× NH), 12.52 (2H, 2× NH). The ^{13}C-NMR spectrum of **HB-3** displayed nine carbon signals with the characteristic carbon of the thione group at δ 178.20 ppm, δ 161.41, 159.92 ppm of two amidic carbonyl groups of the thiobarbituric moiety with one of the higher chemical shifts due to the anisotropic effect of the π-bonds of the furan ring. The mass spectrum of **HB-3** gave a molecular ion peak m/z at 442.44.

The new biphenyl dyes **HB-5–8** (Scheme 2) were prepared *via* condensation reaction of biphenyl-4,4′-dicarbaldehyde (**9**) with cyanoacetic acid (**4**), barbituric acid (**5a**), thiobarbituric acid (**5b**), in methanol–acetic acid as a solvent with reflux. Dye **HB-8** was prepared by refluxing dialdehyde **9** with 4-(2-cyanoacetamido)benzoic acid (**6**) in ethanol as a solvent and piperidine as a catalyst. The biphenyl-dialdehyde **9** was made *via* a Suzuki coupling reaction of 4-bromobenzaldehyde (**7**) with the 4-formylphenylboronic acid (**8**).

3.1.1 Structural characterization. Structures of the newly synthesized dyes **HB-1–4** were assigned based on their elemental and spectral analyses. IR spectra of **HB-1** and **HB-4** displayed the stretching vibrations of nitrile groups at 2228 cm^{-1} (**HB-1**) and 2204 cm^{-1} (**HB-4**), respectively. The stretching vibrations of the O–H group were recorded at 3423 cm^{-1} (**HB-1**) and 3405 cm^{-1} (**HB-4**/OH & N–H). The ^{1}H-NMR spectrum of **HB-1** showed the related protons of the furan ring at δ 7.13, as well as δ 7.62 ppm (two protons each) as two doublet signals with a coupling constant of $J = 4.00$ Hz, and

two singlet signals δ 8.12 (2H, methine-H's), δ 13.88 (2H, carboxylic-H's). The ^{13}C-NMR spectrum of **HB-1** displayed eight carbon signals with the characteristic carbon of the carboxylic group at δ 163.44 ppm. Furthermore, mass analysis of **HB-1** gave a molecular ion peak at $m/z = 324.25$, confirming its molecular weight. The ^{1}H-NMR spectrum of **HB-3** showed the related protons for the furan ring at δ 7.58 and 8.62 ppm (two protons each) with a coupling constant of $J = 4.00$ Hz, and three singlet signals δ 8.03 (2H, methine-H's), δ 12.46 (2H, 2× NH), 12.52 (2H, 2× NH). The ^{13}C-NMR spectrum of **HB-3** displayed nine carbon signals with a characteristic carbon of the thione group at δ 178.20 ppm, δ 161.41, and 159.92 ppm of two amidic carbonyl groups of the thiobarbituric moiety with one of higher chemical shift due to the anisotropic effect of the π-bonds of the furan ring. The mass spectrum of **HB-3** gave a molecular ion peak at $m/z = 442.44$. Furthermore, spectral analysis confirmed the structures of **HB-5–8**. The IR spectra of **HB-5** and **HB-8** displayed the stretching vibrations of nitrile groups at 2221 cm^{-1} (**HB-5**) and 2208 cm^{-1} (**HB-8**), plus OH stretching vibrations at 3321 cm^{-1} (**HB-5**) and 3369 cm^{-1} (**HB-8**/OH & NH). The ^{1}H-NMR spectrum of **HB-5** in DMSO-d_6 displayed the signals of a phenyl ring at δ 7.97, as well as 8.09 ppm (four protons each) with a coupling constant value $J = 8.00$ Hz, and the methine protons (2H) appeared at δ 8.20 ppm. There was also one broad singlet signal of carboxylic protons exchangeable with D$_2$O. The ^{13}C-NMR spectrum of **HB-5** displayed seven carbon signals with the characteristic carbon of the carboxylic group at δ 163.17 ppm. Interestingly, the mass spectrum fragmentation pattern of **HB-5** (Fig. S20†) gave peaks at $m/z = 344$, and $m/z = 300$ *via* loss of carbon dioxide, followed by the loss of another molecule of carbon dioxide to form a fragment at m/z 256.
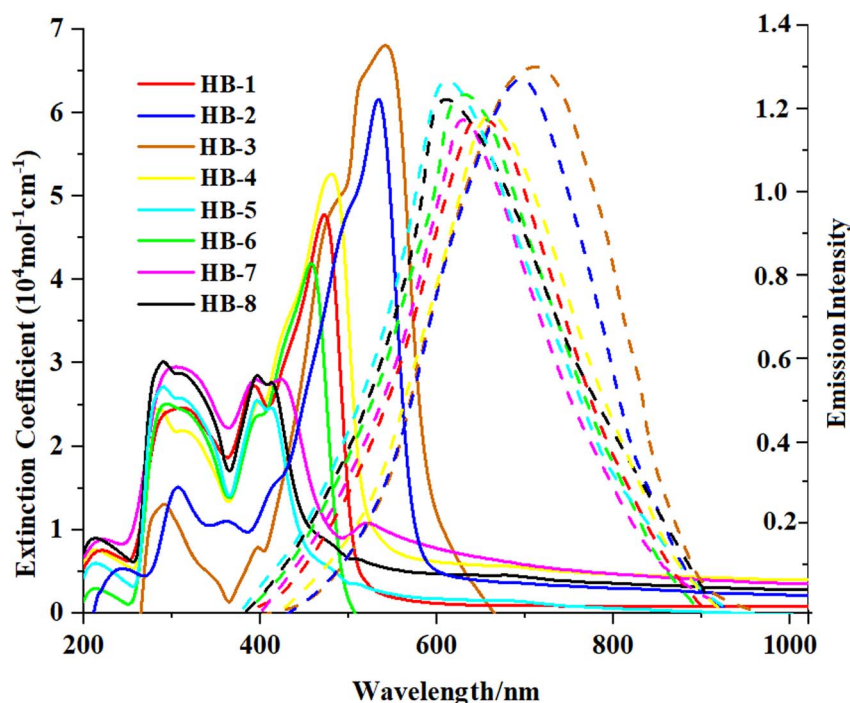

Fig. 2 UV-vis absorption (solid-line) and emission spectra (dashed-line) of **HB-1–8** measured in DMF.

3.2. Optical properties

The absorption spectra of **HB-1–8** were exposed in DMF solution and are shown in Fig. 2. The resultant values are revealed in Table 1. The absorption spectra of the standard dye **N3** is presented in the ESI (Fig. S30†).

Fig. 2 shows the UV-vis absorption spectra of **HB-1–8** in DMF (2×10^{-5} M), and Table 1 describes the findings. The chromophore's $\pi–\pi^*$ electron transition is responsible for the bands appearing in the shorter-wavelength regions. Meanwhile, an intramolecular charge transfer (ICT) occurs from the donors to their associated acceptors and is reflected by an absorption band from 410 to 595 nm.[19] The maximum absorption wavelengths (λ_{max}) were recorded for **HB-1–8** with the increasing order **HB-3** > **HB-2** > **HB-4** > **HB-1** > **HB-6** > **HB-7** > **HB-8** > **HB-5**. From the emission spectra, it is clear that the dyes show strong luminescence maxima in the region of 616–617 nm. The optical band gap was also calculated from the intersection between the normalized absorption and emission spectra.[20] The maximum absorption of **HB-3** with the furan and thiobarbituric acid had a bathochromic-shift of 39 nm relative to that of **HB-2** with the barbituric acid acceptor, and it was red-shifted by the same amount relative to that of **HB-7** with the biphenyl donor and the same acceptor.[21] The reason for this is the improved electron delocalization caused by the π-conjugated sensitizer, as well as

the use of furan as a linker in this D–π framework. Therefore, these data demonstrate that **HB-3** has superior light-harvesting capabilities compared to the other investigated bifuran and biphenyl sensitizers. Additionally, the emission spectra of **HB-1–8** were recorded in DMF (2×10^{-5} M), and their corresponding spectra are shown in Fig. 2. The corresponding data are displayed in Table 1.

We have also recorded the absorption spectra for when the dyes are adsorbed to the TiO$_2$, as illustrated in Fig. 3. Unlike the absorption spectra in DMF, the **HB-1–4** sensitizers had broader absorption bands and blue shifts, which is beneficial to light-harvesting, as well as the J_{SC} value.[22] The formation of the H-type aggregation, in particular, is responsible for the blue shift caused by the bifuran dyes' intense interactions with the semiconductor surface.[23] When compared to the spectral responses of other organic dyes in DMF solution, **HB-5–8** exhibited red-shifted spectra that can be explained by the interaction of the anchoring groups of the dyes with the surface of TiO$_2$, and the stronger tendency to form a J-type aggregation on the TiO$_2$ surface.[24] It is clear that the absorption range before 350–600 nm is compensated well. So, the difference in number and type of anchoring groups in the dyes may result in a different arrangement of the dyes on the surface of TiO$_2$.[25] **HB-3** has a broadening absorption spectrum, indicating better

Table 1 Optical parameters for HB-1–8

Sensitizer	λ_{abs} (nm)	ε (10^4 M^{-1} cm^{-1})	λ_{em} (nm)	Experimental, E_{0-0}[a] (eV)
HB-1	(316, 465)	(2.41, 4.84)	640	2.44
HB-2	(285, 508)	(1.51, 6.13)	710	2.21
HB-3	(293, 547)	(1.30, 6.73)	716	2.11
HB-4	(290, 484)	(2.50, 5.24)	645	2.33
HB-5	(287, 410)	(2.80, 2.53)	614	2.73
HB-6	(294, 459)	(2.51, 4.17)	636	2.52
HB-7	(314, 431)	(2.93, 2.69)	641	2.61
HB-8	(293, 417)	(3.01, 2.37)	616	2.64

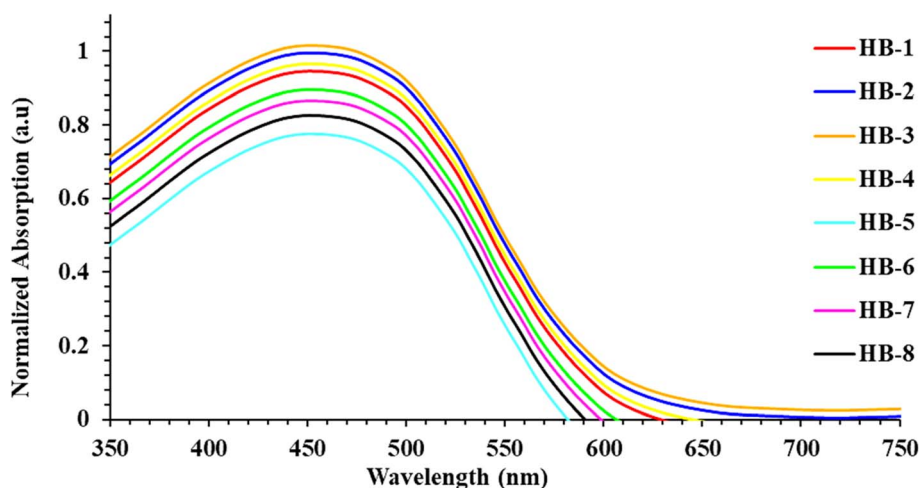[a] E_{0-0} were calculated from the intersection between the absorption and emission profiles.

Fig. 3 Absorption spectra of bifuran/biphenyl dyes **HB-1–8** adsorbed on nonporous TiO$_2$.

characteristics for the short current value (J_{SC}). The presence of the H-aggregate in the device initiated by dye **HB-3** leads to a decrease in the **HB-3** sensitizer's *π energy level, and thus broadens its absorption spectrum.[25] When compared to other dyes and **N3**, **HB-5** had the lowest absorbance, which is determined by the strength of the anchoring and acceptor groups. The absorption profile of **N3** over TiO$_2$ is introduced in the ESI (Fig. S31†).

3.3. Interaction with the TiO$_2$ surface

Therefore, in this paper, we use a combination of FT-IR spectroscopy and density functional theory (DFT) calculations to explore the various anchoring modes onto the TiO$_2$ surface.[26] In addition to simulating the IR spectra of the surface-adsorbed species, we consider monodentate and bidentate binding modes and compare their relative energies at different theoretical levels (Fig. S32 in the ESI†). In the FT-IR spectra of **HB-1** and **HB-5**, notable peaks at 2228 and 2221 cm^{-1} stretching and 1728 and 1751 cm^{-1} stretching were observed. These peaks correlate to (–CN and –CO) and indicate that the cyano and carbonyl groups of the COOH units are linked to the surface of TiO$_2$, as shown in their IR spectra adsorbed to a TiO$_2$ film. Additionally, the FT-IR spectra of bis-barbituric acid-containing **HB-2** and **HB-6** after being anchored on TiO$_2$ rule out physisorption, and point to the dye being chemisorbed onto the TiO$_2$ surface through bidentate binding modes involving the carbonyl and NH groups with the emergence of new peaks. Furthermore, the binding type may be determined by using the Deacon and Phillips assumptions of vibrational frequency study.[27] Anchoring groups participate in dye adsorption by either bidentate chelation or abridging of the top titanium ions,

as shown by the frequency shifts in the NH and CO bands seen for **HB-3** and **HB-7**, both of which contain thiobarbituric acid. The **HB-4** and **HB-8** sensitizers followed the same pattern. Furthermore, there was a shift in frequency for the (NH), (CN), and (CO) bands, suggesting that the cyanoacetamide groups play a role in the dye-adsorption process (Fig. S33–S40†).

3.4. Electrochemical properties

The process for the injection of the electrons into TiO$_2$ and the regeneration of the electrons represent essential behavior in DSSCs. So, the use of cyclic voltammetry (CV) experiments, which is the primary criterion for selecting organic dyes for DSSC applications, has allowed researchers to better understand these processes, as shown in Fig. S41 in ESI.† The excited state oxidation potential (ESOP) is estimated by eqn (1)[28] as follow:

$$\text{ESOP} = [(\text{GSOP (eV)} + 4.7) - E_{0-0}] \text{ eV} \tag{1}$$

The position of the HOMO and the LUMO within the molecular structure of the dye is essential for the performance in DSSCs. The energy of the LUMO level must be greater than the energy potential of the semiconductor (TiO$_2$), so that electrons can spontaneously enter the semiconductor. The dye HOMO level must be lower in energy than the redox potential of the electrolyte (-5.2 eV) that facilitates the retention of the electron back to the dye. As shown in Fig. 4 and Table 2, the HOMO levels obtained for the dyes are in the order **HB-3** (-5.41 eV) > **HB-2** (-5.61 eV) > **HB-4** (-5.74 eV) > **HB-1** (-5.88 eV) > **HB-6** (-6.00 eV) > **HB-7** (-6.13 eV) > **HB-8** (-6.18 eV) > **HB-5** (-6.28 eV), compared to (-4.20 eV) for the conduction band of TiO$_2$.[29] From the data, **HB-3**'s HOMO is higher than the electrolyte
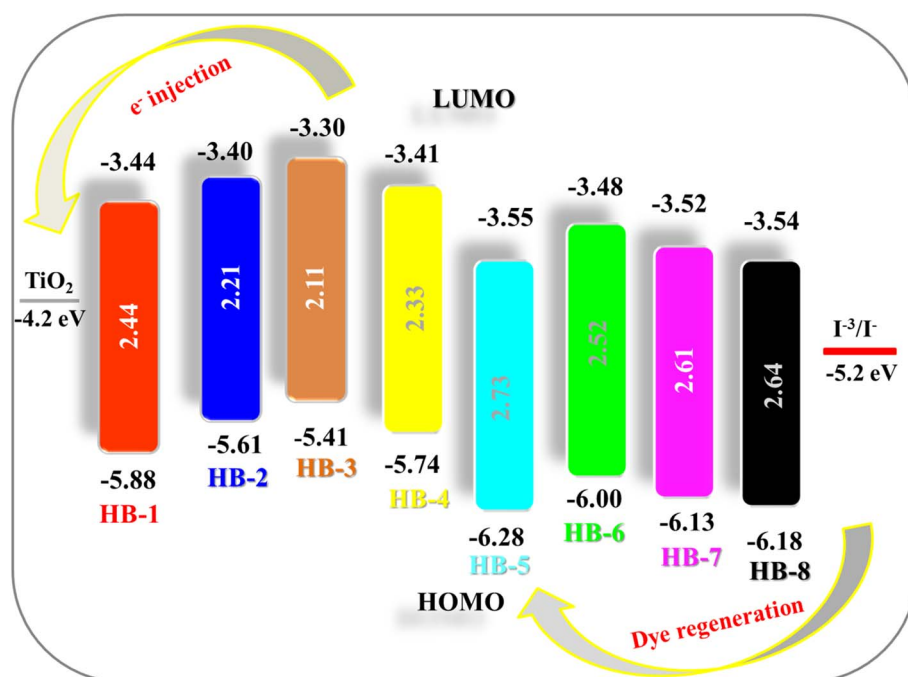

Fig. 4 Energy level diagram for the bifuran/biphenyl sensitizers **HB-1–8**.
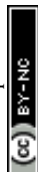

Table 2 Experimental and calculated results (DFT) of (E_{0-0}), HOMO and LUMO for **HB-1–8**

Dye	Experimental (eV)							Calculated (eV)		
	E_{0-0}	HOMO	LUMO	E_{onset}^{oxd}	ΔG_{inj}	ΔG_{rec}	ΔG_{reg}	E_{0-0}	HOMO	LUMO
HB-1	2.44	−5.88	−3.44	1.18	−0.76	−1.68	−0.68	2.43	−5.85	−3.42
HB-2	2.21	−5.61	−3.40	0.91	−0.80	−1.41	−0.41	2.20	−5.60	−3.40
HB-3	2.11	−5.41	−3.30	0.71	−0.90	−1.21	−0.21	2.02	−5.41	−3.39
HB-4	2.33	−5.74	−3.41	1.04	−0.79	−1.54	−0.54	2.31	−5.74	−3.43
HB-5	2.73	−6.28	−3.55	1.58	−0.65	−2.08	−1.08	2.75	−6.25	−3.50
HB-6	2.52	−6.00	−3.48	1.30	−0.72	−1.80	−0.80	2.53	−5.96	−3.43
HB-7	2.61	−6.13	−3.52	1.40	−0.68	−1.93	−0.93	2.64	−6.09	−3.45
HB-8	2.64	−6.18	−3.54	1.48	−0.66	−1.98	−0.98	2.67	−6.14	−3.47

potential, indicating a stronger and more efficient reduction force for the oxidized dye. So, it is plausible that the thiobarbituric acid acceptors present in the **HB-3** dye might improve the device efficiency of **HB-3** relative to that of other dyes.[30] Furthermore, **HB-3** gives the most negative LUMO level (−3.30 eV), indicating that the electron injection process from the excited dye molecule to the TiO_2 conduction band is more efficient for **HB-3**. The schematic energy levels of the bifuran/biphenyl sensitizers **HB-1–8** based on the absorption and electrochemical data are shown in Fig. 4.

Understanding the various thermodynamic processes that occur at the dye/electrolyte/semiconductor interfaces is critical for designing an efficient device.[31] The driving forces, ΔG_{inj}, ΔG_{rec}, and ΔG_{reg}, were calculated to gain insight into the viability of dye injection, recombination, and regeneration processes by using eqn (2)–(4).

$$\Delta G_{inj}\ (eV) = E_{OX}^{dye*} - E_{CB} \qquad (2)$$

$$\Delta G_{rec}\ (eV) = E_{OX}^{dye} - E_{CB} \qquad (3)$$

$$\Delta G_{reg}\ (eV) = E_{OX}^{dye} - E_{redox} \qquad (4)$$

As can be observed from the data, all of the ΔG values obtained are negative, indicating the thermodynamic

feasibility of all of the aforementioned processes.[32] Based on the electrochemical data obtained, it is possible to conclude that **HB-3** is a potential dye with greater electron injection feasibility than recombination. The values of ΔG_{inj} of **HB-1–8** were found to be as follows: **HB-3** (−0.90 eV) > **HB-2** (−0.80 eV) > **HB-1** (−0.76 eV) > **HB-4** (−0.81 eV) > **HB-6** (−0.72 eV) > **HB-7** (−0.68 eV) > **HB-8** (−0.66 eV) > **HB-5** (−0.65 eV). Based on the above results, it seems that the di-anchoring **HB-3** has the highest ΔG_{inj} value (−0.90 eV) compared to the other studied sensitizers, which permits it to inject electrons more effectively into TiO_2's CB.[33] **HB-3** also had the highest ΔG_{rec} value, indicating that it has superior recombination resistance, which can be influenced by the presence of di symmetric anchoring moieties. Furthermore, all of the bifuran/biphenyl sensitizers **HB-1–8** were shown to have sufficient driving force G_{reg} values for their regeneration process in order to prevent recombination between the photo-oxidized state and injected electrons, resulting in a higher cell J_{SC} value.[34] Also, the ΔG_{reg} value of (−1.21 eV) for **HB-3** indicates the highest performance of the dye due to the better regeneration of the oxidized dye. Based on the electrochemical data obtained, it is possible to conclude that the sensitizer **HB-3** is a potential dye with greater electron injection and recombination feasibility.
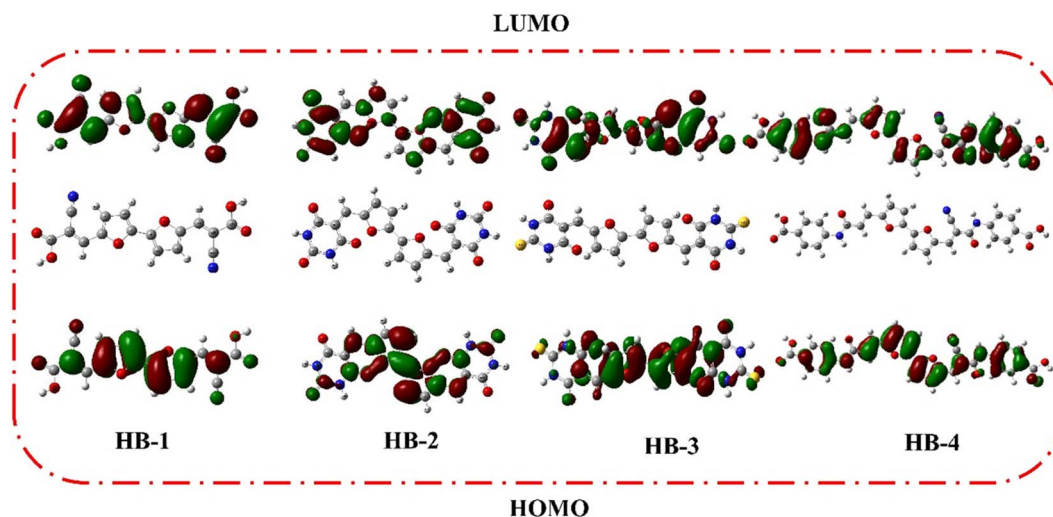
Fig. 5 HOMOs and LUMOs for bifuran sensitizers **HB-1–4**.

3.5. Molecular modeling

DFT calculations were performed on bifuran/biphenyl sensitizers **HB-1–8** by the B3LYP/6–311G using Gaussian09 software to gain insight into the molecular structure of the dyes, as depicted in Fig. 5.[35] The optimized molecular configurations and charge density dispersion at their FMO energies are shown in Fig. 5. The HOMO levels of **HB-1–4** show that the electron cluster is concentrated chiefly on the furan moiety, which then precisely moved from an electron-donating substituent to electron acceptors (cyanoacetic acid, barbituric acid, thiobarbituric acid, and 4-carboxylcyanoacetamide) at their LUMO levels, but this occurred to varying degrees for each of these compounds because of their specific electron-receiving properties. The symmetric bifuran substituent of **HB-3** has HOMO, and the LUMO electron density is completely localized on the anchoring thiobarbituric acid substituent, as shown by the findings; this allows for electronic interactions between the LUMO electron density and the TiO_2 d-orbitals, and the coexistence between the HOMO and LUMO levels guarantees a rapid photo-induced transfer of electrons from the donating part to the acceptor group. Because of this increased charge separation, **HB-3** has a much higher photovoltaic efficiency than other sensitizers.

From Fig. 6, the HOMO for **HB-5–8** is randomly distributed throughout the framework, whereas the LUMOs were located in the anchoring parts (barbituric, thiobarbituric acid units) through the biphenyl-spacer. For **HB-5–8**, this means that the LUMO electron destination does not really tightly coincide with TiO_2's conduction band (CB), which could lead to poor electron injection efficiency from the dyes' LUMO.

3.6. Molecular electrostatic potential (MEP)

Molecular electrostatic potentials (MEP) **HB-1–8** dyes help to understand the molecular orbital behavior.[36] As shown in Fig. S42 in the ESI,† the negative (red) low potentials are located on the carbonyl group and cyano group for **HB-1** and **HB-6**, but

located for the carbonyl of the barbituric moiety for **HB-2** and **HB-7**. For **HB-3** and **HB-7** containing thiobarbituric acid as acceptor, it is localized over the carbonyl group. In contrast, the donating components, like the bifuran and biphenyl regions, are in the MEP map's blue positive zone, suggesting that they are good candidates for nucleophilic attack. Analyzing the MEP of the **HB-1–8** bichalcophene sensitizers' surfaces reveals how many free electrons are available to interact with other atomic species. Based on this finding, we may infer the composition of the ICT in all **HB-1–8** sensitizers after adsorption on TiO_2.

4. Photovoltaic device characterizations

The photocurrent density–photovoltage (J–V) curves of the DSSCs based on **HB-1–8** compared to **N3** are shown in Fig. 7, and the key parameters including short-circuit current density (J_{SC}), open-circuit voltage (V_{OC}), fill factor (FF) and overall power conversion efficiency (η) are summarized in Table 3. It is clear that the photovoltaic performances of the DSSCs can be clearly affected by the anchoring group in the dye molecules. The PCE increases in the order of **N3** (5.61%) > **HB-3** (5.51%) > **HB-2** (5.00%) > **HB-4** (4.07%) > **HB-1** (3.96%) > **HB-6** (3.50%) > **HB-7** (3.44%) > **HB-8** (2.93%) > **HB-5** (2.91%). Under the same conditions, the cells sensitized with **HB-1–8** and **N3** gave increasing J_{SC} in the following order: **N3** (18.22) > **HB-3** (17.84) > **HB-2** (16.73) > **HB-4** (15.72) > **HB-1** (15.43) > **HB-6** (14.73) > **HB-7** (13.73) > **HB-8** (12.93) > **HB-5** (12.13) mA cm^{-2} and V_{OC} **HB-3** (515) > **N3** (505) > **HB-2** (460) > **HB-4** (459), **HB-1** (459) > **HB-6** (441) > **HB-7** (440) > **HB-8** (421) > **HB-5** (420) mV, respectively. Among the bifuran/biphenyl **HB-1–8** dyes, **HB-3** outperforms the other dyes in solar cell performance, especially in J_{SC} and V_{OC}, because of its strong anchoring property with TiO_2, which facilitated the injection of electrons into the TiO_2 surface.[37] The increased J_{SC} value of **HB-3** in comparison to the other bifuran/biphenyl dyes is primarily attributable to its relatively superior light harvesting capability
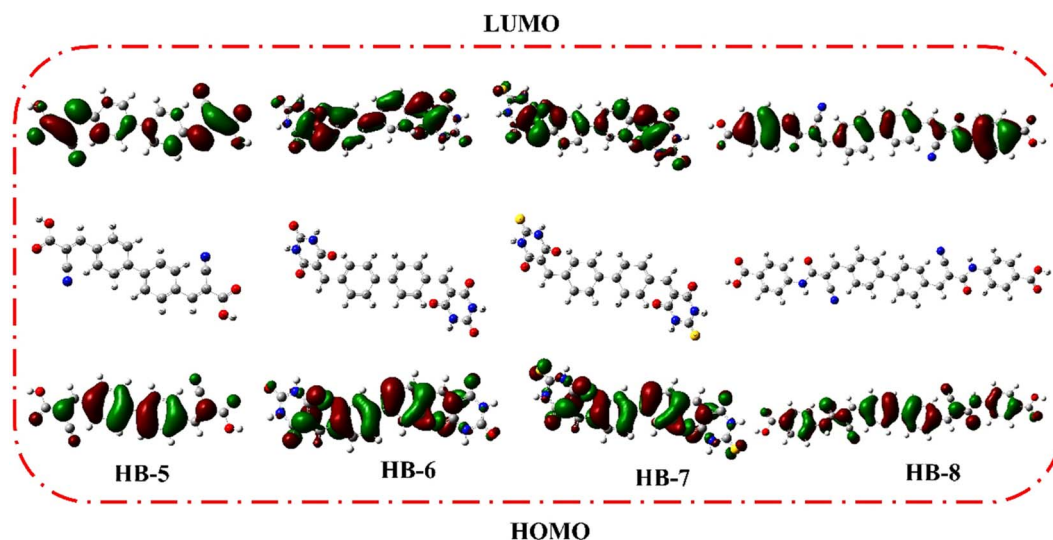

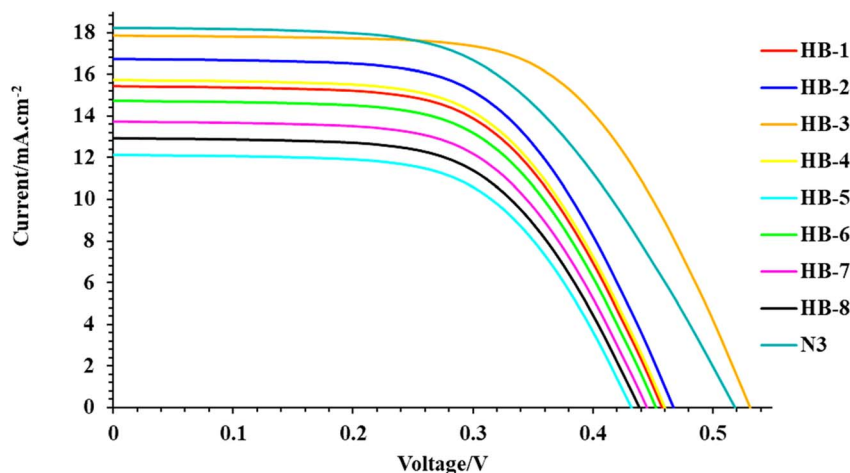**Fig. 6** HOMOs and LUMOs for biphenyl sensitizers HB-5−8.

Fig. 7 $J-V$ curves of bifuran/biphenyl sensitizers **HB-1–8** and **N3**.

Table 3   Photovoltaic parameters data for **HB-1–8**

Sensitizer (0.2 mM)	V_{OC} (mV)	J_{SC} (mA cm^{-2})	FF	η (%)
N3	505	18.22	0.61	5.61
HB-1	459	15.43	0.56	3.96
HB-2	460	16.73	0.65	5.00
HB-3	515	17.84	0.60	5.51
HB-4	459	15.72	0.56	4.07
HB-5	420	12.13	0.57	2.90
HB-6	441	14.73	0.54	3.50
HB-7	440	13.73	0.57	3.44
HB-8	421	12.93	0.54	2.93

(broad absorption spectrum and high molar extinction coefficient), which is reflected in its superior IPCE spectrum.[37] Compared to **N3** dyes, **HB-3** had significantly higher V_{OC} values, indicating that its thiobarbituric acid group has a high tendency to inject electrons from the LUMO to the TiO$_2$ conduction band.

The reason for this is that the bulky **N3** dye adsorbs poorly on the semiconductor surface, producing bigger spaces in between the attached organic molecules.[38]

However, when compared to other sensitizer-based devices, **HB-5** exhibited the lowest V_{OC} and J_{SC} values. This may be primarily due to the poor interaction between the sensitizer and TiO$_2$, resulting in the lowest efficiency.

Fig. 8 displays the wavelength dependence of the incident photon-to-electron conversion efficiency (IPCE) for fabricated cells using the four dyes as photosensitizers. Fig. 8 shows that the IPCE of the bifuran/biphenyl sensitizers is greater than 40% within the wavelength scale from 410 to 520 nm; **HB-5** exhibited a significant value of 57.6% at 500 nm. Dye **HB-1–8** sensitizers have narrower IPCE spectra than **N3**, resulting in lower photocurrent and lower photovoltaic effectiveness.[39] The relatively higher IPCE for **HB-3** in comparison to other dyes is consistent with the UV-vis absorption properties' tendency.[40] In comparison, **HB-1–4** bearing a bifuran attached to various acceptor moieties exhibits a broader IPCE spectrum compared to **HB-5–8**
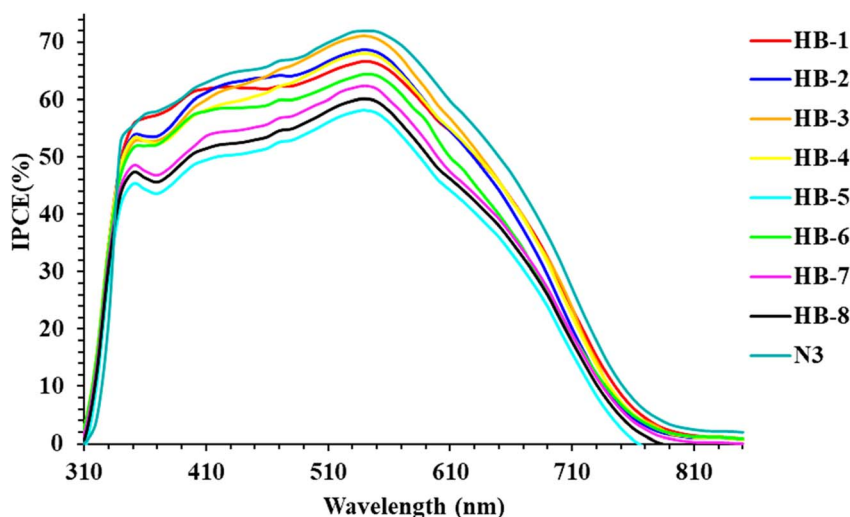

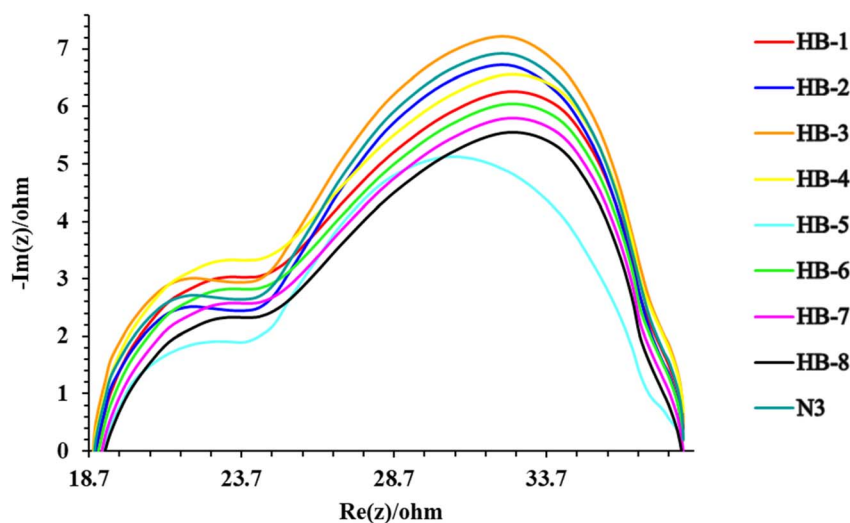Fig. 8   IPCE spectra of bifuran/biphenyl sensitizers **HB-1–8** and **N3**.

Fig. 9 EIS Nyquist plot for bifuran/biphenyl sensitizers **HB-1–8** and **N3**.

containing a biphenyl with various acceptors. The **HB-3** sensitized TiO$_2$ electrodes achieve the maximum conversion yield among the investigated bifuran/biphenyl dyes due to their higher and broader IPCE values than those of the other sensitizers in the remaining region.

4.1. Electrochemical impedance spectroscopy (EIS)

Electrochemical impedance spectroscopy (EIS) measurements were performed to characterize the charge transfer resistances of the cells. Fig. 9 shows the electrochemical impedance spectra for the DSSCs based on the three sensitizers (**HB-1–8**). EIS experiments were carried out to assess the interfacial charge recombination and carrier transit mechanisms in the manufactured DSSCs.[41,42] The Nyquist plots of the DSSCs made with sensitizers **HB-1–8** and **N3** are shown in Fig. 9. In the Nyquist plots of the sensitized devices, two semicircles were demonstrated, and it was interesting to note that the radius of the second semicircle of the produced DSSCs was found to be in the order: **HB-3** > **N3** > **HB-2** > **HB-4** > **HB-1** > **HB-6** > **HB-7** > **HB-8** > **HB-5**. According to the results, **HB-3** plays a crucial role in reducing the overall dark current/back response in the sensitized DSSCs. Based on the V_{OC} levels associated with the manufactured cells listed in Table 3, the aforementioned result is consistent.

5. Conclusion

We have synthesized, described, and implemented new bifuran/biphenyl derivatives that contain cyanoacetic acid, barbituric acid, thiobarbituric acid, and 4-carboxylcyanoacetamide acceptors in dye-sensitized solar cells. As a result of thiobarbituric acid's electron-withdrawing ability, **HB-3** dye has the biggest maximum absorption wavelength and maximum molar absorption coefficient. In comparison to other dyes, the DSSC based on **HB-3** with bifuran and thiobarbituric units has a higher average conversion efficiency (5.51%). In comparison to other dyes, DSSCs based on **HB-3** with the bifuran and

thiobarbituric units have a higher average conversion efficiency (5.51%). DSSCs based on bifuran/biphenyl sensitizers showed good conversion efficiencies and short-circuit currents that are consistent with the electrochemical impedance spectroscopy results. The photovoltaic performance is highly variable depending on the electron-acceptors in the organic sensitizers.

Data availability

The data supporting the findings of this study are available on request from the corresponding author.

Author contributions

Conflicts of interest

The authors declare no conflict of interest, financial or otherwise.

Acknowledgements

References

1 M. Grätzel, *Nature*, 2001, **414**, 338–344.
2 D. Luo, W. Jang, D. D. Babu, M. S. Kim, D. H. Wang and A. K. K. Kya, *J. Mater. Chem. A*, 2022, **10**, 3255–3295.
3 M. Grätzel, *J. Photochem. Photobiol., C*, 2003, **4**, 145–153.

4 M. K. Nazeeruddin, A. Kay, I. Rodicio, R. Humphry-Baker, E. Müller, P. Liska, N. Vlachopoulos and M. Grätzel, *J. Am. Chem. Soc.*, 1993, **115**, 6382–6390.

5 A. M. Aldusi, A. A. Fadda, M. A. Ismail and M. R. Elmorsy, *Appl. Organomet. Chem.*, 2022, e6893.

6 L. Lyu, R. Su and A. El-Shafei, *ChemistrySelect*, 2022, **7**, e202202183.

7 P. S. Gangadhar, A. Jagadeesh, M. N. Rajesh, A. S. George, S. Prasanthkumar, S. Soman and L. Giribabu, *Mater. Adv.*, 2022, **3**, 1231–1239.

8 C. Liao, H. Wu, H. Tang, L. Wang and D. Cao, *Sol. Energy*, 2022, **240**, 399–407.

9 J. Zou, Y. Tang, G. Baryshnikoy, Z. Yang, R. Mao, W. Feng, J. Guan, C. Li and Y. Xie, *J. Mater. Chem. A*, 2022, **10**, 1320–1328.

10 R. Grisorio, L. De Marco, G. Allegretta, R. Giannuzzi, G. P. Suranna, M. Manca and G. Gigli, *Dyes Pigm.*, 2013, **98**(2), 221–231.

11 F. H. Abdelhamed, M. A. Ismail, E. Abdel-Latif, A. A. Abdel-Shafi and M. R. Elmorsy, *J. Mater. Sci.: Mater. Electron.*, 2022, 1–14.

12 B.-Y. Zhu, L. Wu, Q. Ye, J.-R. Gao and L. Han, *Tetrahedron*, 2017, **73**, 6307–6315.

13 X. Ren, S. Jiang, M. Cha, G. Zhou and Z. S. Wang, *Chem. Mater.*, 2012, **24**, 3493.

14 S. Jiang, S. Fan, X. Lu, G. Zhou and Z. S. Wang, *J. Mater. Chem. A*, 2014, **2**, 17153–17164.

15 X. Ren, S. Jiang, M. Cha, G. Zhou and Z. S. Wang, *Chem. Mater.*, 2012, **24**, 3493–3499.

16 R. Sirohia, D. H. Kim, S. C. Yu and S. H. Lee, *Dyes Pigm.*, 2012, **92**, 1132.

17 B. Taljaard and G. J. Burger, *Adv. Synth. Catal.*, 2002, **344**, 1111–1114.

18 S. Dwivedi, S. Bardhan, P. Ghosh and S. Das, *RSC Adv.*, 2014, **4**, 41045–41050.

19 C. X. Xia, N. Wang, P. P. Sun, S. X. Tang, X. D. Xu, Y. B. Tan and X. Xin, *Soft Matter*, 2020, **16**, 7390–7399.

20 G. Wu, F. Kong, Y. Zhang, X. Zhang, J. Li, W. Chen and S. Dai, *Dyes Pigm.*, 2014, **105**, 1–6.

21 B. Hosseinzadeh, A. S. Beni, A. N. Chermahini, R. Ghahary and A. Teimouri, *Synth. Met.*, 2015, **209**, 1–10.

22 M. R. Elmorsy, R. Su, E. Abdel-Latif, S. A. Badawy, A. El-Shafei and A. A. Fadda, *J. Mater. Sci.: Mater. Electron.*, 2020, **31**, 7981–7990.

23 G. Wu, F. Kong, Y. Zhang, X. Zhang, J. Li, W. Chen, C. Zhang and S. Dai, *Dyes Pigm.*, 2014, **105**, 1–6.

24 R. Sanchez-de-Armas, M. A. San Miguel, J. Oviedo and J. F. Sanz, *Phys. Chem. Chem. Phys.*, 2012, **14**, 225–233.

25 B. Hosseinzadeh, A. S. Beni, A. N. Chermahini, R. Ghahary and A. Teimouri, *Synth. Met.*, 2015, **209**, 1–10.

26 N. A. Wazzan, *J. Comput. Electron.*, 2019, **18**, 375–395.

27 L. da Silva, M. Sánchez, M. Ibarra-Rodriguez and H. S. Freeman, *J. Mol. Struct.*, 2021, **1250**, 131749.

28 M. R. Elmorsy, S. A. Badawy, E. Abdel-Latif, M. A. Assiri and T. E. Ali, *Dyes Pigm.*, 2023, **214**, 111206.

29 B.-Y. Zhu, L. Wu, Q. Ye, J.-R. Gao and L. Han, *Tetrahedron*, 2017, **73**, 6307–6315.

30 J. Xu, L. Zhang, J. Chen, P. Shen, M. Ye, N. Y. Yuan and J. N. Ding, *Thin Solid Films*, 2018, **645**, 129–133.

31 M. Pazoki, U. B. Cappel, E. M. J. Johansson, A. Hagfeldt and G. Boschloo, *Energy Environ. Sci.*, 2017, **10**, 672–709.

32 R. Kesavan, F. Attia, R. Su, P. Anees, A. El-Shafei and A. V. Adhikari, *J. Phys. Chem. C*, 2019, **123**, 24383–24395.

33 K. Sun, Y. Ma, W. Zhang, Y. Wen, L. Wang and J. Zhang, *Dyes Pigm.*, 2017, **139**, 148–156.

34 X. Zarate, F. Claveria-Cadiz, D. Arias-Olivares, A. Rodriguez-Serrano, N. Inostroza and E. Schott, *Phys. Chem. Chem. Phys.*, 2016, **18**, 24239–24251.

35 M. Lundberg, T. Kawatsu, T. Vreven, M. J. Frisch and K. Morokuma, *J. Chem. Theory Comput.*, 2009, 222–234.

36 M. R. Elmorsy, E. Abdel-Latif, H. E Gaffer, S. A. Badawy and A. A. Fadda, *J. Mol. Struct.*, 2022, **1255**, 132404.

37 J. Zhang, H.-C. Zhu, R.-L. Zhong, L. Wang and Z.-M. Su, *Org. Electron.*, 2018, **54**, 104–113.

38 Y.-J. Chen, Y.-C. Chang, L.-Y. Lin, W.-C. Chang and S.-M. Chang, *Electrochim. Acta*, 2015, **178**, 414–419.

39 K. S. Keremane, A. Planchat, Y. Pellegrin, D. Jacquemin, F. Odobel and A. V. Adhikari, *ChemSusChem*, 2022, **15**, e202200520.

40 P. Naik, R. Su, M. R. Elmorsy, A. El-Shafei and A. V. Adhikari, *Dyes Pigm.*, 2018, **149**, 177–187.

41 G. Oskam, B. V. Bergeron, G. J. Meyer and P. C. Searson, *J. Phys. Chem. B*, 2001, **105**, 6867–6873.

42 Y. Hua, B. Jin, H. Wang, X. Zhu, W. Wu, M.-S. Cheung, Z. Lin, W.-Y. Wong and W.-K. Wong, *J. Power Sources*, 2013, **237**, 195–203.